Focused Ion Beam milling and MicroED structure determination of metal-organic framework crystals

Andrey A. Bardin[a,b], Alison Haymaker[a,b], Fateme Banihashemi[a,], Jerry Y.S. Lin[a], Michael W. Martynowycz[c,*], and Brent L. Nannenga[a,b,*]

[a]Chemical Engineering, School for Engineering of Matter, Transport and Energy, Arizona State University, Tempe, AZ, USA

[b]Biodesign Center for Applied Structural Discovery, Biodesign Institute, Arizona State University, 727 East Tyler Street, Tempe, AZ 85287, USA

[c]Department of Biological Chemistry, University of California, Los Angeles CA 90095

*Corresponding Authors: Email: Brent.Nannenga@asu.edu (B.L.N.), mikewm@g.ucla.edu (M.M)

Abstract

We report new advancements in the determination and high-resolution structural analysis of beam-sensitive metal organic frameworks (MOFs) using microcrystal electron diffraction (MicroED) coupled with focused ion beam milling at cryogenic temperatures (cryo-FIB). A microcrystal of the beam-sensitive MOF, ZIF-8, was ion-beam milled in a thin lamella approximately 150 nm thick. MicroED data were collected from this thin lamella using an energy filter and a direct electron detector operating in counting mode. Using this approach, we achieved a greatly improved resolution of 0.59 Å with a minimal total exposure of only 0.64 e^-/A^2. These innovations not only improve model statistics but also further demonstrate that ion-beam milling is compatible with beam-sensitive materials, augmenting the capabilities of electron diffraction in MOF research.

1. Introduction

Metal-organic frameworks (MOFs) continue to attract attention in material science due to their diverse applications, from gas storage to catalysis [1]. These porous materials have a three-dimensional structure, often consisting of metal ions or clusters coordinated to organic ligands, and they are particularly renowned for their large surface areas. Within this family, Zeolitic Imidazolate Frameworks (ZIFs) offer unique benefits, including chemical robustness, scalable synthesis, and varied topologies. ZIF-8, characterized by its sodalite (SOD) topology, serves as a model system, given its particular relevance for storage and separation tasks [2]. ZIF-8 is frequently utilized due to its stability and flexibility in various applications. The use of X-ray crystallography has been the key tool for high-resolution structure determination of MOFs [3], however this is dependent on the growth of large crystals that can be difficult for many samples.

As an alternative, transmission electron microscopy (TEM) has thus proven invaluable for studying MOFs as TEM accommodates micro and nanocrystals, sidestepping the need for the larger crystals typically demanded by X-ray methods. While high-resolution TEM imaging and electron diffraction methods have been successfully used on MOFs [4-8], the beam-sensitive nature of many MOFs, such as ZIF-8, poses challenges. To help overcome this hurdle, TEM's low-dose imaging and cryogenic settings can be used to mitigate radiation damage. Microcrystal electron diffraction (MicroED), a specialized cryoEM technique within the TEM umbrella [9, 10], brings additional advantages. This methodology has been applied to a wide variety of samples, from biological macromolecules to small molecules and materials. MicroED employs ultra-low electron doses and cryogenic conditions to preserve the native state of beam-sensitive samples and reduce the effects of radiation damage [11]. Coupled with rapid data collection and electron counting cameras, these features facilitate high-resolution structure determination while minimizing radiation-induced alterations. MicroED was previously applied to ZIF-8, resulting in a 0.87Å structure from a single nanocrystal, thereby demonstrating the applicability of the technique to the study of beam sensitive MOFs [12]. While imaging and diffraction-based TEM methods are powerful tools for MOF structure determination, a key limitation is the requirement for very thin samples. For example, the

previous MicroED study on ZIF-8 made use of a crystal that was approximately 200 nm in diameter to produce the high-resolution structure, where ZIF-8 crystals that were larger (400 – 800 nm) produced lower quality data [12]. This constraint on crystal thickness can be particularly problematic for the cases where crystals are too thick for electron diffraction data collection, yet still too small for X-ray crystallography.

To advance the use of electron diffraction methodologies on the study of MOF structure further, we sought to incorporate the use of focused ion beam milling (FIB) under cryogenic temperatures (cryo-FIB) into the MicroED structure determination workflow to control crystal thickness. FIB milling has generally been used in semiconductor manufacturing and materials science for site-specific analysis, deposition, and ablation of materials. The use of FIB milling for sensitive samples is often thought to be too damaging for high-resolution studies. However, recently it has been shown that the use of cryo-FIB milling can facilitate high-resolution imaging of MOF samples up to 1.2 Å [13, 14]. For macromolecular crystallography, coupling cryo-FIB milling of crystals with MicroED analysis for high-resolution structure determination has become a powerful approach, with several recent studies using these methods [15-19]. However, this approach has not yet been demonstrated for electron diffraction of organic frameworks.

In this work we have applied cryo-FIB milling to reduce ZIF-8 microcrystals, approximately 15 µm in size, to lamellae roughly 150 nm thick. This preparation step optimizes the crystals for MicroED data collection. Additionally, we incorporate an energy filter with a 5 eV width and employ a Falcon 4i direct electron detector in counting mode to improve data quality. Together these enhancements led to a resolution of 0.59 Å, an improvement from our previous 0.87 Å ZIF-8 structure and was achieved with an ultra-low exposure of only 0.64 e^-/A^2. Importantly, this study verifies that cryo-FIB milling, previously instrumental in improving MicroED data quality for macromolecular crystals, can be applied effectively to MicroED analysis of non-biological, beam-sensitive materials without inducing significant damage. These advancements extend the applicability of these methods to a wider range of materials science challenges. We present methodological advancements in this work that further establish electron diffraction as a primary choice for high-resolution structure determination of beam-sensitive MOFs and

ZIFs. This paves the way for broader applicability and sets a new benchmark for data collection protocols that open new avenues for materials otherwise limited by traditional methods.

2. Methods

2.1 ZIF-8 synthesis

The ZIF-8 crystals were synthesized with modifications to the previously reported method [20]. The synthesis started with the preparation of two solutions, one by dissolving 0.505 g of zinc chloride ($ZnCl_2$, Sigma-Aldrich, 98.0%)) in 25 mL of methanol, and another containing 0.608g of 2-methylimidazole (2-MeIm) and 0.505 g of $NaHCO_2$ (Sigma-Aldrich, 99.0%) in the same amount of methanol. The solutions were mixed separately and then the 2-MeIm solution was poured into the $ZnCl_2$ solution under stirring. The solution with a molar ratio of 1 Zn: 2 2-MeIm: 2 $NaHCO_2$: 333 MeOH was transferred to a Teflon-lined stainless-steel autoclave in a preheated convection oven at 130°C for 4 h under homogeneous heating. The resultant crystals were then separated from the colloidal solution by three cycles of centrifugation (6000 rpm, 15 min) and washed with methanol under ultrasound. The morphology and crystallographic properties of ZIF-8 crystals were examined using scanning electron microscopy (SEM, Amray 1910) and X-ray powder diffraction (XRD, Malvern PANalytical Aeris) with a scan step of 0.015°.

2.2 ZIF-8 sample preparation and ion beam milling

ZIF-8 crystals suspended in methanol were deposited on 200 mesh holey carbon grids by pipetting 3 µL of the crystalline suspension onto the carbon surface of the grid. The grids carrying ZIF-8 crystals we allowed to dry to remove excess methanol and then were placed under vacuum in a cryogenically cooled ThermoFisher Aquilos dual beam focused ion-beam and scanning electron microscope (FIB/SEM) for milling into thin lamellae. We followed protocols detailed previously [21]. Initially, the grids were sputter-coated under fine and coarse settings for a minute each, thus adding a layer of conducting platinum to aid SEM imaging and protect the crystals from the gallium ion beam. Subsequently, a

protective layer of approximately 500 nm of organic platinum volatile was applied to the grids using a gas injection system. Crystals meeting specific criteria (not located on a grid bar, within two grid squares of the grid edge) were identified via SEM and FIB imaging. Prior to milling, these identified crystals were moved to the eucentric position.

The milling process consisted of four steps: trenching, rough milling, fine milling, and polishing. Trenching was performed with a 1nA beam current over an area of about 10 µm, extending approximately 10 µm above and below the desired lamellae position. The trenching stage concluded when a lamella of around 5 µm thickness was obtained. Rough milling followed, using a 300pA current, to reduce the lamella to a thickness of 1 µm and its width to around 9 µm. During the fine milling stage, a 100pA current was employed to bring the lamella down to a final thickness of 400-500 nm and a width of approximately 8 µm. Lastly, polishing was done at a 30pA milling current until the lamella was between 150-200 nm thick and 5-7 µm wide. This procedure was implemented on five selected sites on the grid using a 30kV accelerating voltage and gallium ions as the liquid metal source. The milled crystalline lamellae were subsequently stored in liquid nitrogen until the MicroED experiments in the cryo-TEM.

2.4 MicroED data collection

For data collection, the grids with milled lamellae were carefully rotated by 90° and transferred into a Titan Krios 3Gi, operating under cryogenic conditions at a 300 kV accelerating voltage. An all-grid atlas was obtained initially to locate the lamellae sites, which are characterized by the appearance of stripes of missing material with a small, semi-transparent substance in the middle. Each site was moved to the eucentric position before MicroED data collection. Data was collected from each site in a 63° wedge over 420 seconds using a Falcon 4i direct electron detector, without employing a beamstop. The smallest C2 aperture of 50 µm was selected, along with a spot size of 11, and a beam diameter of 30 µm to reduce crystal exposure and enable data collection without a beamstop. The diffraction data were gathered from a small region of the crystal (≈ 2 µm in diameter) using a selected area aperture. Any inelastic signal was removed using a Selectris energy filter with a 5 eV slit width. The data was recorded in MRC format,

generating 840 4k x 4k frames in total, where each frame represented approximately 0.075° of data.

2.5 Data processing and structure determination

The collected MicroED data was first transformed from MRC to SMV format utilizing the microed-tools software, which is available at cryoem.ucla.edu. This data was then subjected to indexing, integration, and scaling using XDS and XSCALE [22]. Data from a single crystal was ultimately used and transformed into the SHELX format for further processing. To determine the structure, we employed SHELXT, and subsequent refinement of the derived structure was performed utilizing SHELXL [23, 24].

3. Results and Discussion

In our previous study, we synthesized ZIF-8 particles to be in the size range of a few hundred nanometers to be directly suitable for MicroED analysis [12]. In this work we focused on synthesizing larger crystals to test the application of cryo-FIB milling on ZIF-8. Following ZIF-8 synthesis, SEM confirmed that the obtained ZIF-8 particles are composed of dispersed crystals of rhombic dodecahedral shape with particle size in the range of 10-30 μm (Fig. 1A). Powder XRD was employed to verify the synthesis of ZIF-8 (Fig 1B), and characteristic diffraction peaks can be seen at 2θ of 7.4°, 10.4°, 12.7°, 14.7°, 16.4°, 18.0°, 22.1°, 24.5°, 26.7° and 29.6°, which can be assigned to the (011), (002), (112), (022), (013), (222), (114), (233), (134) and (044) planes respectively. These prominent reflections agree well with the sodalite structure of ZIF-8 in XRD patterns reported in literature [25, 26].

The ZIF-8 crystals were applied to the surface of a holey carbon grid from the methanol suspension essentially as described in our previous work with the ZIF-8 nanocrystals [12]. One key difference here is that we made use of 200 mesh holey carbon grids rather than 300 mesh grids to reduce the number of copper grid bars and increase the usable area of the grid for cryo-FIB milling. Following the evaporation of the methanol, the ZIF-8 grids were loaded into the cryo-FIB/SEM for milling. When the sample was

visualized within the FIB/SEM, many ZIF-8 crystals could be seen on the surface (Fig. 2A). There were several features of the crystals on the grid that were assessed to determine if a crystal was suitable for milling. These included, crystal morphology (single crystal, well-defined shape), located near the center of the grid square away from grid bars, and no other crystals in the path of the ion beam. Crystals that fit these criteria were selected for FIB milling and thin lamella (≈ 150nm thick) were created from these crystals (Fig. 2B).

The milled crystals were next analyzed in the cryo-TEM by MicroED. Initial electron diffraction patterns collected from the thinned lamella produced very high-resolution diffraction, with diffraction spots extending to beyond 0.6Å (Fig. 2C), indicating that the lamella did not experience significant FIB damage. Because of the beam sensitivity of these crystals, ultra-low doses were used, with the final exposure of only 0.64 e^-/A^2 per data set. This represents a reduction of approximately 36% relative to the previous ZIF-8 study. The ability to both reduce dose and still obtain higher resolution data was largely due to the use of a more sensitive direct electron detector in this study. MicroED data sets were collected from the crystalline lamella, and ultimately data from a single crystal was used to determine the structure of ZIF-8 from a FIB-milled crystal to 0.59 Å (Fig. 3, Table 1).

The data collected from the single lamella yielded a processed dataset that was 98.9% complete and direct methods were used to solve the structure of the FIB milled ZIF-8 sample. After several rounds of structure refinement, the final structure closely resembles previous ZIF-8 structures determined by X-ray crystallography and electron diffraction [12, 27-29]. The crystal was in space group I-43m with each MeIM molecule interacting with two zinc atoms through the ligand's nitrogen atoms. Each zinc is coordinated by a total of 4 different MeIM ligands to form the zeolite structure (Fig 3). In the structure, volume of the solvent accessible voids is 2,323 $Å^3$ (48.7% of unit cell volume). This high-resolution MicroED structure of ZIF-8 further demonstrates that cryo-FIB milling can preserve high resolution features even when working with sensitive samples. Previous cryo-FIB milling work on MOFs using high-resolution TEM showed that images in the range of 1.2 to 2.0 Å could still be obtained [13, 14]. This study demonstrates that quality

structural information to at least 0.59 Å is still preserved after cryo-FIB milling of beam-sensitive MOF crystals.

4. Conclusion

This work presents the first-ever structure of an ion-beam milled MOF determined by MicroED. It demonstrates that ion beam milling can be effectively used together with MicroED on small molecules and MOFs. By employing thin lamellae extracted from microcrystals that are conventionally challenging to study—either too small for X-ray diffraction or too thick for traditional electron diffraction—this approach promises to overcome existing methodological constraints when using electron diffraction for structure determination in the field of chemical crystallography and facilitate structure determination across a wider range of materials and sizes.

When compared to our previous report on ZIF-8 from unmilled nanocrystals [12], data quality enhancements in this study are primarily attributable to a synergistic amalgamation of technologies: the transition from CetaD to Falcon 4i direct electron detectors, the integration of ion beam milling, and the incorporation of a 5 eV energy filter. These collective improvements have sharpened both crystallographic statistics and resolution, establishing a new benchmark for MOF data collection. Looking ahead, further advances in MicroED technology promise to extend its capabilities. The use of Cold FEG (Field Emission Gun) could enhance electron beam coherency [30, 31]. The advent of faster or more sensitive electron detectors would refine data acquisition [32]. Innovations like plasma focused ion beam milling and lower milling energies could yield samples with even less surface damage, thereby opening the door for improved data quality and new structures [33]. Additionally, the potential to selectively analyze different regions of the milled MOF lamella opens exciting avenues. This could allow for the study of the population and spatial distribution of guest molecules within MOFs, yielding invaluable insights into their function and efficacy.

Together, this work demonstrates the power of coupling cryo-FIB milling and MicroED methodologies for the study of MOF structure. Future work and optimization promise

enhance structure quality and throughput, leading to new understanding and discoveries in small molecule crystallography and the study of organic frameworks.

Data availability

Coordinates for ZIF-8 have been deposited in the Cambridge Structural Database (CCDC 2284295)

Acknowledgements

JYSL would like to acknowledge support from the National Science Foundation (CBET-1511005 and CBET-2031087). BLN would like to acknowledge the support from the National Science Foundation (DMR-1942084). BLN and MWM acknowledge support from the National Institutes of Health (P41GM136508).

Figures

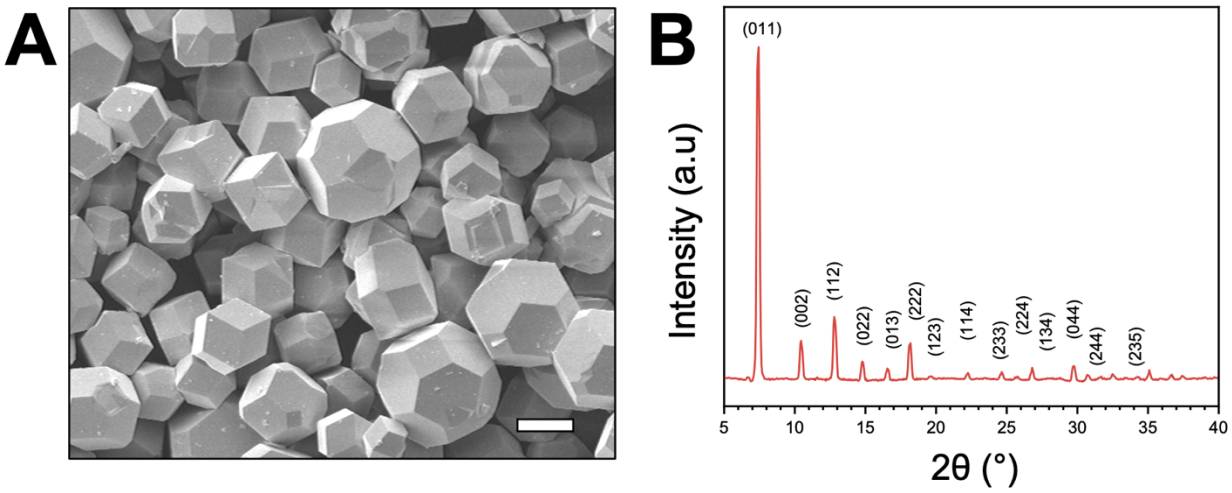

Figure 1. SEM micrograph (A) and XRD pattern (B) of synthesized ZIF-8 microcrystals. Scale bar in A represents 10 μm.

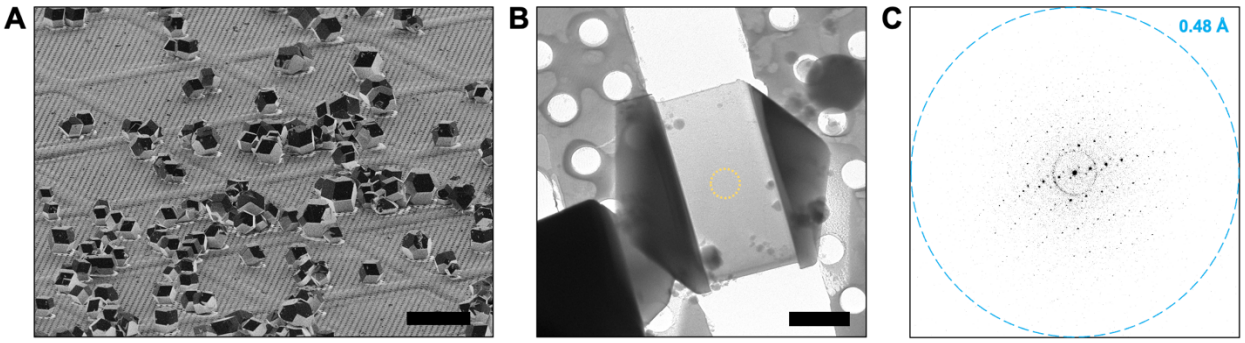

Figure 2. Cryo-FIB miling and MicroED data collection of ZIF-8 crystals. (A) An ion beam image in the cryo-FIB/SEM shows ZIF-8 crystals dispersed on the surface of the holey carbon grid. (B) Following FIB milling of the crystals, the thin lamella could be identified in the cryo-TEM and used for MicroED data collection. The exposed area of the crystals is indicated by the yellow circle (approximately 2 μm in diameter). Scale bars in A and B represent 50 and 4 μm, respectively. (C) Representative frames from the MicroED data set of the milled ZIF-8 crystal used for structure determination.

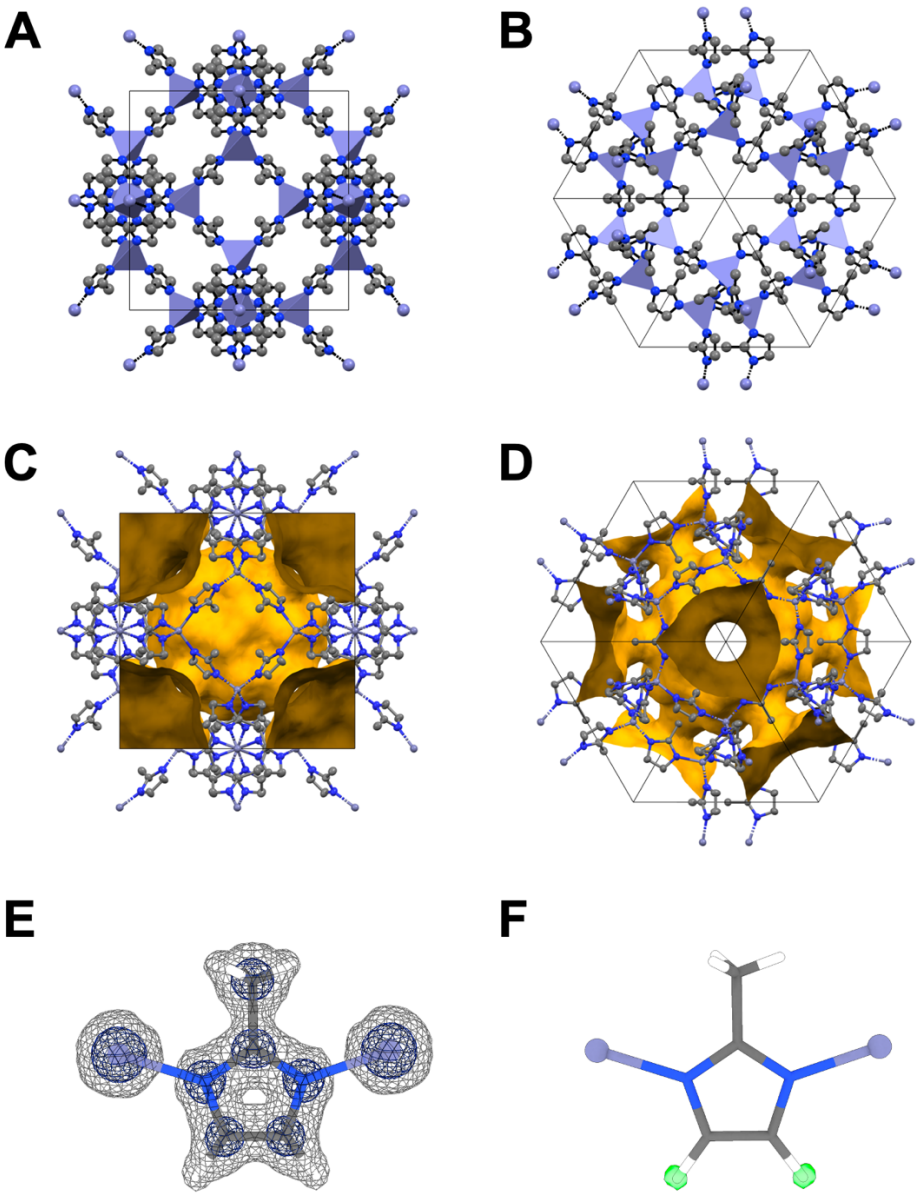

Figure 3. MicroED structure of FIB-milled ZIF-8. (A-D) The crystal structure determined from the crystalline lamella viewed along the (100) (A, C) and the (111) (B, D) directions, with the void volumes displayed in panels C and D. Hydrogen atoms are omitted for clarity in panels A-D. (E,F) The potential maps show clear features, demonstrating the quality of the MicroED collected from the FIB-milled crystal. The F_{obs} maps in E are contoured at 3σ (Blue) and 1σ (gray). When hydrogens are omitted, the $F_{obs} – F_{calc}$ map (F) shows positive density (green, 3σ) for the imidazole hydrogen. The density is less visible for the methyl hydrogens as there is disorder at this position, which is modeled, but not shown in the figure for clarity.

Table 1. Data collection and refinement statistics

	ZIF-8
Data collection	
Excitation Voltage	300 kV
Wavelength (Å)	0.019687
Number of crystals	1
Data Processing	
Space group	I-43m
Unit cell length a = b = c (Å)	16.830
Angles α = β = γ (°)	90.00
Resolution (Å)	11.90 - 0.59
Number of reflections	8,275 (887)
Unique reflections	1,200 (127)
R_{obs} (%)	10.7 (64.0)
R_{meas} (%)	11.7 (69.1)
I/σ_I	8.47 (1.40)
$CC_{1/2}$ (%)	99.6 (45.2)
Completeness (%)	98.9 (90.7)
Structure Refinement	
R1 (%)	11.09
wR2 (%)	36.97
GooF	1.200

Values in parentheses represent numbers in the highest resolution shell (0.62 – 0.59 Å)

References

[1] H.C. Zhou, J.R. Long, O.M. Yaghi, Introduction to metal-organic frameworks, Chem Rev, 112 (2012) 673-674.

[2] C. Zhang, R.P. Lively, K. Zhang, J.R. Johnson, O. Karvan, W.J. Koros, Unexpected molecular sieving properties of zeolitic imidazolate framework-8, The journal of physical chemistry letters, 3 (2012) 2130-2134.

[3] F. Gandara, T.D. Bennett, Crystallography of metal–organic frameworks, IUCrJ, 1 (2014) 563-570.

[4] X. Gong, K. Gnanasekaran, Z. Chen, L. Robison, M.C. Wasson, K.C. Bentz, S.M. Cohen, O.K. Farha, N.C. Gianneschi, Insights into the Structure and Dynamics of Metal–Organic Frameworks via Transmission Electron Microscopy, Journal of the American Chemical Society, 142 (2020) 17224-17235.

[5] S. Yuan, J.-S. Qin, H.-Q. Xu, J. Su, D. Rossi, Y. Chen, L. Zhang, C. Lollar, Q. Wang, H.-L. Jiang, D.H. Son, H. Xu, Z. Huang, X. Zou, H.-C. Zhou, [Ti8Zr2O12(COO)16] Cluster: An Ideal Inorganic Building Unit for Photoactive Metal–Organic Frameworks, ACS Central Science, 4 (2018) 105-111.

[
6] D. Lenzen, J. Zhao, S.-J. Ernst, M. Wahiduzzaman, A. Ken Inge, D. Fröhlich, H. Xu, H.-J. Bart, C. Janiak, S. Henninger, G. Maurin, X. Zou, N. Stock, A metal–organic framework for efficient water-based ultra-low-temperature-driven cooling, Nature Communications, 10 (2019) 3025.

[7] M. Ge, Y. Wang, F. Carraro, W. Liang, M. Roostaeinia, S. Siahrostami, D.M. Proserpio, C. Doonan, P. Falcaro, H. Zheng, X. Zou, Z. Huang, High-Throughput Electron Diffraction Reveals a Hidden Novel Metal-Organic Framework for Electrocatalysis, Angew Chem Int Ed Engl, 60 (2021) 11391-11397.

[8] Z. Meng, C.G. Jones, S. Farid, I.U. Khan, H.M. Nelson, K.A. Mirica, Unraveling the Electrical and Magnetic Properties of Layered Conductive Metal-Organic Framework With Atomic Precision, Angewandte Chemie International Edition, 61 (2022) e202113569.

[9] B.L. Nannenga, T. Gonen, The cryo-EM method microcrystal electron diffraction (MicroED), Nat Methods, 16 (2019) 369-379.

[10] M.T.B. Clabbers, A. Shiriaeva, T. Gonen, MicroED: conception, practice and future opportunities, IUCrJ, 9 (2022) 169-179.

[11] L.A. Baker, J.L. Rubinstein, Chapter Fifteen - Radiation Damage in Electron Cryomicroscopy, in: G.J. Jensen (Ed.) Methods Enzymol, Academic Press, 2010, pp. 371-388.

[12] F. Banihashemi, G. Bu, A. Thaker, D. Williams, J.Y.S. Lin, B.L. Nannenga, Beam-sensitive metal-organic framework structure determination by microcrystal electron diffraction, Ultramicroscopy, 216 (2020) 113048.

[13] L. Liu, D. Zhang, Y. Zhu, Y. Han, Bulk and local structures of metal–organic frameworks unravelled by high-resolution electron microscopy, Communications Chemistry, 3 (2020) 99.

[14] J. Zhou, N. Wei, D. Zhang, Y. Wang, J. Li, X. Zheng, J. Wang, A.Y. Alsalloum, L. Liu, O.M. Bakr, Y. Han, Cryogenic Focused Ion Beam Enables Atomic-Resolution Imaging of Local Structures in Highly Sensitive Bulk Crystals and Devices, Journal of the American Chemical Society, 144 (2022) 3182-3191.

[15] H.M.E. Duyvesteyn, A. Kotecha, H.M. Ginn, C.W. Hecksel, E.V. Beale, F. de Haas, G. Evans, P. Zhang, W. Chiu, D.I. Stuart, Machining protein microcrystals for structure determination by electron diffraction, Proceedings of the National Academy of Sciences, 115 (2018) 9569-9573.

[16] H. Alison, A.B. Andrey, G. Tamir, W.M. Michael, L.N. Brent, Structure determination of a DNA crystal by MicroED, bioRxiv, (2023) 2023.2004.2025.538338.

[17] M.W. Martynowycz, M.T.B. Clabbers, J. Hattne, T. Gonen, Ab initio phasing macromolecular structures using electron-counted MicroED data, Nat Methods, 19 (2022) 724-729.

[18] M.W. Martynowycz, A. Shiriaeva, X. Ge, J. Hattne, B.L. Nannenga, V. Cherezov, T. Gonen, MicroED structure of the human adenosine receptor determined from a single nanocrystal in LCP, Proceedings of the National Academy of Sciences, 118 (2021) e2106041118.

[19] M.W. Martynowycz, F. Khan, J. Hattne, J. Abramson, T. Gonen, MicroED structure of lipid-embedded mammalian mitochondrial voltage-dependent anion channel, Proceedings of the National Academy of Sciences, 117 (2020) 32380.

[20] J. Cravillon, C.A. Schröder, H. Bux, A. Rothkirch, J. Caro, M. Wiebcke, Formate modulated solvothermal synthesis of ZIF-8 investigated using time-resolved in situ X-ray diffraction and scanning electron microscopy, CrystEngComm, 14 (2012) 492-498.

[21] M.W. Martynowycz, T. Gonen, Protocol for the use of focused ion-beam milling to prepare crystalline lamellae for microcrystal electron diffraction (MicroED), STAR Protoc, 2 (2021) 100686.

[22] W. Kabsch, Xds, Acta Crystallogr D Biol Crystallogr, 66 (2010) 125-132.

[23] G.M. Sheldrick, SHELXT - integrated space-group and crystal-structure determination, Acta Crystallogr A Found Adv, 71 (2015) 3-8.

[24] G.M. Sheldrick, Crystal structure refinement with SHELXL, Acta Crystallogr C Struct Chem, 71 (2015) 3-8.

[25] Y. Pan, Y. Liu, G. Zeng, L. Zhao, Z. Lai, Rapid synthesis of zeolitic imidazolate framework-8 (ZIF-8) nanocrystals in an aqueous system, Chemical Communications, 47 (2011) 2071-2073.

[26] Y. Zhang, Y. Jia, L.a. Hou, Synthesis of zeolitic imidazolate framework-8 on polyester fiber for PM2.5 removal, RSC Advances, 8 (2018) 31471-31477.

[27] K.S. Park, Z. Ni, A.P. Côté, J.Y. Choi, R. Huang, F.J. Uribe-Romo, H.K. Chae, M. O'Keeffe, O.M. Yaghi, Exceptional chemical and thermal stability of zeolitic imidazolate frameworks, Proceedings of the National Academy of Sciences, 103 (2006) 10186.

[28] W. Morris, C.J. Stevens, R.E. Taylor, C. Dybowski, O.M. Yaghi, M.A. Garcia-Garibay, NMR and X-ray Study Revealing the Rigidity of Zeolitic Imidazolate Frameworks, The Journal of Physical Chemistry C, 116 (2012) 13307-13312.

[29] H.T. Kwon, H.-K. Jeong, A.S. Lee, H.S. An, J.S. Lee, Heteroepitaxially Grown Zeolitic Imidazolate Framework Membranes with Unprecedented Propylene/Propane Separation Performances, Journal of the American Chemical Society, 137 (2015) 12304-12311.

[30] T. Nakane, A. Kotecha, A. Sente, G. McMullan, S. Masiulis, P.M.G.E. Brown, I.T. Grigoras, L. Malinauskaite, T. Malinauskas, J. Miehling, T. Uchański, L. Yu, D. Karia, E.V. Pechnikova, E. de Jong, J. Keizer, M. Bischoff, J. McCormack, P. Tiemeijer, S.W. Hardwick, D.Y. Chirgadze, G. Murshudov, A.R. Aricescu, S.H.W. Scheres, Single-particle cryo-EM at atomic resolution, Nature, 587 (2020) 152-156.

[31] K.M. Yip, N. Fischer, E. Paknia, A. Chari, H. Stark, Atomic-resolution protein structure determination by cryo-EM, Nature, 587 (2020) 157-161.

[32] B.D.A. Levin, Direct detectors and their applications in electron microscopy for materials science, Journal of Physics: Materials, 4 (2021) 042005.

[33] M.W. Martynowycz, A. Shiriaeva, M.T.B. Clabbers, W.J. Nicolas, S.J. Weaver, J. Hattne, T. Gonen, A robust approach for MicroED sample preparation of lipidic cubic phase embedded membrane protein crystals, Nature Communications, 14 (2023) 1086.